Conformational Differences Between *C*- and *O*-Glycosides: The α-*C*-Mannobiose/α-*O*-Mannobiose Case

Juan-Félix Espinosa,[a] Marta Bruix,[b] Olivier Jarreton,[c] Troels Skrydstrup,[c,d] Jean-Marie Beau,[c] and Jesús Jiménez-Barbero*[a]

Abstract: The conformational behavior of methyl α-*C*-mannobiose (**1**) and an analogue **3** bearing a hydroxy group at the bridging position have been studied with a combination of NMR spectroscopy (*J* and NOE data) in different solvents and molecular mechanics and dynamics calculations. The obtained results show clear differences with respect to the *O*-disaccharide analogue **2**.

Keywords: conformation analysis · *C*-glycosides · mannobiose · molecular modeling

Introduction

In recent years the search for new glycosidase inhibitors has led to a group of oligosaccharide analogues with the glycosidic oxygen substituted by carbon.[1] In fact, *C*-glycosides may serve as carbohydrate mimics resistant to metabolic processes.[2] Nevertheless, for *C*-disaccharides to be biologically useful, it is required that their conformational behavior should be analogous to that of the natural compound. Therefore, it is important to determine how the synthetic derivatives behave. Kishi and coworkers have been very active in this field, and solely on the basis of a semiquantitative analysis of NMR data, mainly coupling constants, have proposed similar conformations for both kinds of compounds.[3] However, their conclusions are somewhat unexpected since the substitution of an oxygen by a methylene group results in a change in both the size and the electronic properties of the glycosidic linkage.[4] Using a combination of NMR (NOE and *J* data) and molecular mechanics, we recently reported for the first time that the assumption of similar conformations for *C*- and *O*-glycosides is not true for *C*- and *O*-lactose (with a β-glycosidic linkage), since the orientation around the aglyconic bond is quite different for the two derivatives.[5] These results have encouraged us to extend our studies to determine whether these findings can be generalized for other carbon-bridged saccharides. The study of a α-linked *C*-disaccharide such as α-*C*-mannobiose[6] would provide new insights on this topic, since owing to the different contributions of *exo*-anomeric and steric effects α-glycosidic bonds may be expected to be conformationally different to β-glycosidic linkages. On this basis, we report here the conformational study of methyl α-*C*-mannobiosides **1** and **3** using a combination of NMR spectroscopy and MM3* molecular mechanics and dynamics calculations.[7] Compound **1** is the *C*-analogue of the disaccharide moiety α-D-Man-(1 $\rightarrow$2)α-D-Man (**2**), a frequently occurring structural motif in a variety of glycoconjugates.[8]

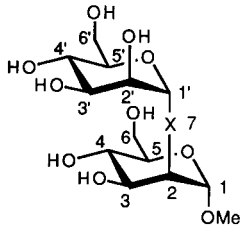

1 X = CH_2
2 X = O
3 X = CHOH

Results and Discussion

Conformation of methyl α-*C*-mannobioside (1) in aqueous solution: The adiabatic surfaces[7] calculated for **1** and **2** are shown in Figure 1. From these energy surfaces, probability distributions were obtained according to a Boltzmann func-

[a] Dr. J. Jiménez-Barbero, Dr. J.-F. Espinosa
Instituto de Química Orgánica, CSIC
Juan de la Cierva 3, E-28006 Madrid (Spain)

[b] Dr. M. Bruix
Instituto de Estructura de la Materia, CSIC
Serrano 119, E-28006 Madrid (Spain)

[c] Dr. O. Jarreton, Assoc. Prof. T. Skrydstrup,[d] Prof. Dr. J.-M. Beau
Université de Paris-Sud
Laboratoire de Synthèse de Biomolécules
URA CNRS 462, Institut de Chimie Moléculaire
F-91405 Orsay Cédex (France)

[d] Current address:
Department of Chemistry
Aarhus University, Langelandsgade 140
DK-8000 Aarhus C (Denmark)

Supporting information for this article is available on the WWW under http://www.wiley-vch.de/home/chemistry/ or from the author.

0947-6539/99/0502-0442 $ 17.50+.50/0 *Chem. Eur. J.* **1999**, *5*, No. 2

Table 1. Torsional angle values (ϕ,ψ) of the predicted minima and MM3* populations (GB/SA solvent model) of the low-energy regions. The regions around ϕ extend for about 20° and around ψ for about 30°.

	C-mannobiose (**1**)			*O*-mannobiose (**2**)		*C*-(OH)-mannobiose (**3**)		
	A	B	C	A	B	A	B	C
torsion angle ϕ/ψ	−68/−52	−48/43	49/47	−52/−25	−44/31	−80/−60	−59/32	60/51
population [%]	15.7	58.8	25.1	80.9	19.1	39.0	7.2	53.8

tion. Glycosidic torsion angles are defined as ϕ H1′-C1′-C7-C2 and ψ C1′-C7-C2-H2. Two different conformational families are found for **2** (Table 1). The global minimum A has dihedral angles of $\phi = -52 \pm 20$ and $\psi = -25 \pm 30$, and about 81% of the population is located around this conformer. This conformation is in agreement with the global minimum previously described using HSEA calculations[9] ($\phi = -47$, $\psi = -20$) and is also in accordance with earlier values for similar linkages.[10] The potential energy surface previously found for **2** is similar to ours. In fact, this map shows a satisfactory fit between experimental (steady-state NOEs and T_1s) and theoretical results.[9]

On the other hand, the analysis of the distribution map for **1** shows clear differences: three conformational families coexist in solution and the global minimum is located in a different region (Figures 1b and 2, minimum B, $\phi = -48 \pm 20$, $\psi = 43 \pm 30$) accounting for 59% of the population. This minimum displays a similar value for the glycosidic torsion in comparison to minimum A (the *exo*-anomeric conformation)[11] but the orientation around the *C*-aglyconic bond is rather different. It is noteworthy that a third conformational family (Figures 1b and 2, minimum C, $\phi = 49 \pm 20$, $\psi = 47 \pm 30$) is predicted with a population of approximately 25%. This conformation does not correspond with the *exo*-anomeric disposition since the C7–C2 bond is *anti* with respect to the C1′–O5′ bond. In fact, this conformation has never been observed for α-*O*-mannobioside moieties. Additional information on the conformational stability of the different minima was obtained from MD simulations with the MM3* force field using the continuum GB/SA (generalized Born solvent-accessible surface area) solvent model for water.[12] Independent of the starting minimum (A, B, or C), the calculated trajectories showed several interconversions among the three different regions. The trajectory bears a clear resemblance to the adiabatic surface described above.

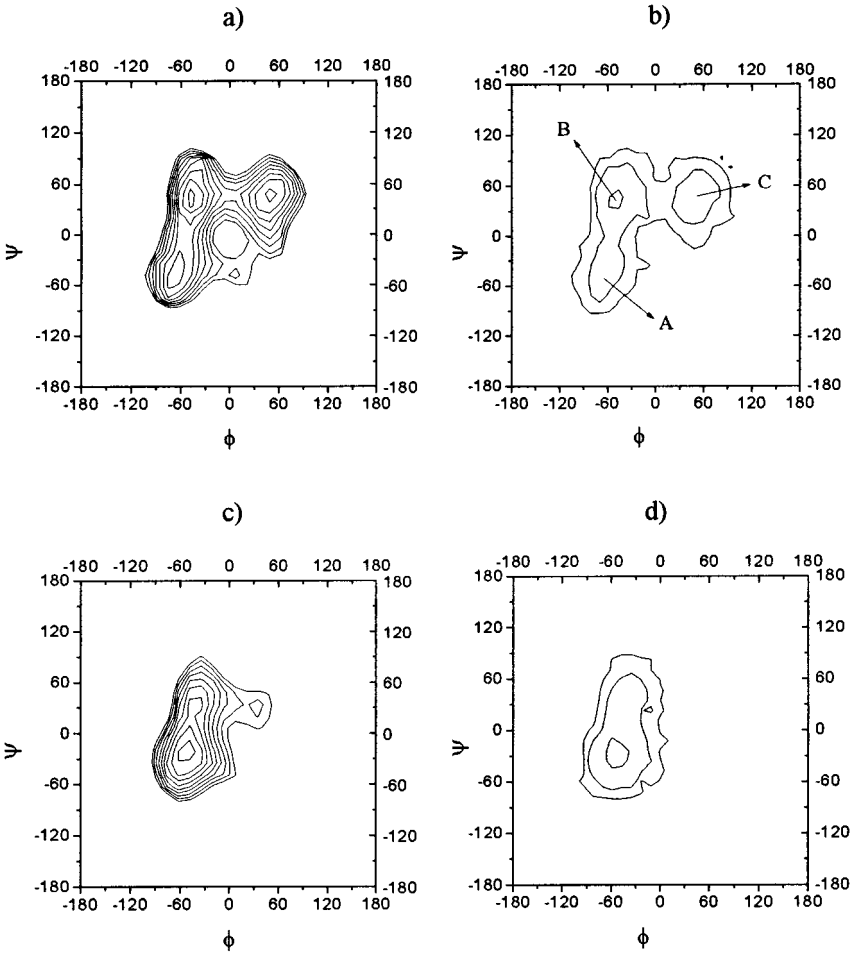

Figure 1. Adiabatic (a,c) and population distribution (b,d) maps for **1** (a,b) and **2** (c,d). Energy contours are given every 0.5 kcal mol^{-1}. Distribution contours are given at 10%, 1% and 0.1% of the population.

The validity of the theoretical results has been tested using NMR measurements of vicinal coupling constants and NOEs. The assignment of the resonances was made through a combination of COSY and TOCSY experiments. Experiments (500 and 600 MHz) were performed at a variety of temperatures to avoid signal overlapping. Second-order analysis of the spectrum was performed to obtain refined δ and J values. The results are shown in Table 2 along with the expected values for all the minima and for the ensemble average,

Abstract in Spanish: *Se ha estudiado, mediante una combinación de RMN y cálculos de mecánica y dinámica molecular, el comportamiento conformacional en disolución del metil α-C-manobiósido (**1**) y de un análogo que presenta un grupo hidroxilo en el carbono interglicosídico (**3**). Los resultados indican claras diferencias respecto al O-disacárido natural (**2**).*

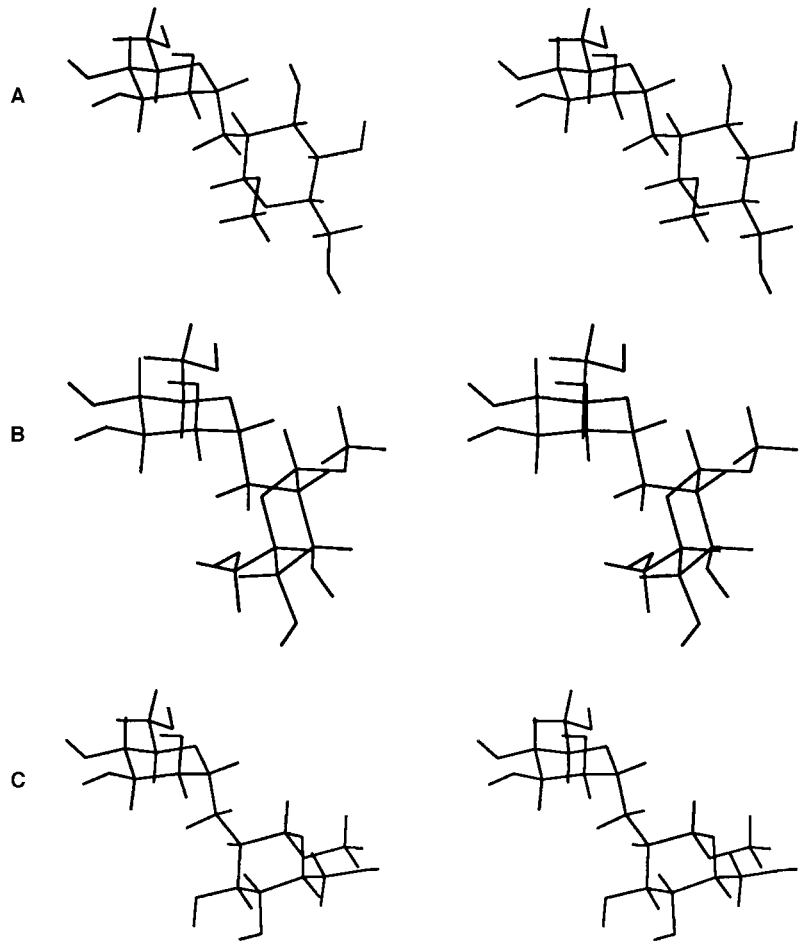

Figure 2. Stereoscopic views of the low-energy conformations obtained by MM3* calculations for compound **1.**

calculated using the Haasnoot – Altona modification of the Karplus equation.[13] Diastereotopic assignment of the prochiral H7pro*R* and H7pro*S* protons was performed, using a combination of *J* and NOE values, as follows. Since the high-field proton shows two large couplings (8.9 and 8.7 Hz to H2 and H1′, respectively), for the major conformer of **1**, this proton (H7*anti*) presents an antiperiplanar relationship to both H2 and H1′. Two sets of torsion angles permit this orientation : ϕ/ψ $-60/60^\circ$ or ϕ/ψ $60/-60^\circ$. In the first case, H7pro*S* would be H7*anti*; for ϕ/ψ $60/-60^\circ$, H7pro*R* would be H7*anti*. Both orientations have exclusive NOEs which can be used to assign the diastereotopic H7 protons. Those NOEs are H1/H5′ and H1/H1′, for the first case, and H4/H2′ for the second one. In addition, the first orientation predicts that the H7*anti*/H1 NOE should be weaker than the H7not-*anti*/H2′ NOE. Experimentally, the presence of both H1/H5′ and H1/H1′ NOEs, the absence of the H4/H2′ NOE, and the stronger intensity of the H7not-*anti*/H2′ NOE with respect to the H7*anti*/H1 NOE leads us to the deduction that H7*anti* is indeed H7pro*S*. It has to be stressed that no computational calculations have been used to reach this conclusion. Nevertheless, the NMR-based assignment is in complete agreement with the calculations which predict no population of the ϕ/ψ $60/-60^\circ$ conformer (see above). Coming back to the conformational analysis of **1**, the four interglycosidic coupling constant values indicate that it is not possible to explain all of them simultaneously with only one minimum, and that the three A, B, and C conformations should be taken into account. The match between theoretical and experimental data using the MM3*-predicted Boltzmann distribution is excellent.

Table 2. Relevant experimental vicinal coupling constants (*J* [Hz] obtained at 600 MHz) across the interglycosidic linkage of **1** and **3** in different solvents. The values expected for the different minima and the ensemble average values are also given. H7pro*R* and H7pro*S* assignments are based on NOE/*J* analysis.

H/H pair	Theoretical values				Experimental values			
	A	B	C	Distribution	D_2O	[D_6]DMSO	[D_5]Pyr	MeOD
H-1′/$H7_{proS}$	11.6	11.2	2.3	8.8	8.7	9.2	9.8	9.3
H1′/$H7_{proR}$	2.7	1.2	11.6	4.0	3.5	3.4	3.3	3.4
H2/$H7_{proS}$	1.9	11.9	11.9	9.7	8.9	9.2	8.6	9.3
H2/$H7_{proR}$	12.3	1.4	1.5	3.5	4.1	3.1	4.7	3.6
H1′/H7 (**3**)	2.6	0.8	9.3	6.0	5.3	–	–	–
H2/H7 (**3**)	11.9	0.2	0.5	6.3	5.3	–	–	–

Further information was obtained from NOE experiments. 2D-NOESY (recorded at 500 and 600 MHz; one example is shown in Figure 3),[14] 2D-ROESY, and 1D-DPFGSE NOESY[15] spectra were acquired. The relevant interresidue proton – proton distances are shown in Table 3. As for the *J*

Table 3. Relevant interresidue and ensemble average $\langle r^{-6}\rangle^{-1/6}$ proton – proton distances. Strong, medium, and weak experimental NOEs are denoted by s, m, and w, respectively.

Proton pair	Min. A	Min. B	Min. C	Ensemble (**1**)	**1** D_2O	**1** [D_6]DMSO	**1** MeOD	**1** [D_5]Pyr	**3** D_2O
	Theoretical values				Experimental values				
H1-H1′	4.7	3.2	2.1	2.6	ms	ms	ms	m	s
H1-H5′	3.4	2.8	5.2	2.9	mw	mw	m	mw	w
H2-H2′	4.7	4.2	2.2	2.8	mw	mw	mw	mw	ms
H2-H5′	2.6	4.3	4.6	3.5	w	w	w	mw	mw
H2-H1′	3.2	2.4	2.9	2.5	s	s	s	s	m

0947-6539/99/0502-0444 $ 17.50+.50/0 *Chem. Eur. J.* **1999**, *5*, No. 2

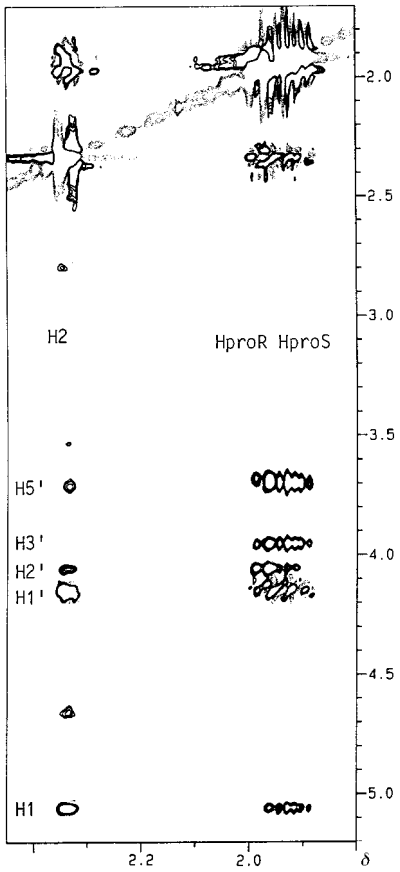

Figure 3. Partial NOESY spectrum of **1** (600 MHz, 303 K, D_2O). There is partial overlap between protons H1′ and H3 and between H5′ and H4.

data, it is not possible to justify simultaneously all the observed NOEs with just one conformer. Qualitatively, the presence of strong NOEs between H1′ and H2 and between H1 and H5′ indicates that the global minimum B is heavily populated in solution. The NOE between H2 and H5′ also points to the presence of conformer A, since this contact is exclusive for this minimum. Finally, the existence of conformer C is also confirmed by NMR data. The distance between H2 and H2′ is greater than 4 Å in both conformer A and conformer B, and is 2.2 Å in conformer C. Therefore, the existence of this H2/H2′ NOE can only be explained by the occurrence of conformer C. From a quantitative point of view, Figure 4 shows the build-up curves for the key NOEs in comparison with the values obtained from the population distribution using a full relaxation matrix approach.[14] It can be observed that the agreement is satisfactory. Nevertheless, the experimentally observed large H2/H2′ and the small H2/H5′ NOEs suggest, respectively, that the population around C is slightly overestimated by the calculations (<25%), whereas the population around A should be larger than the predicted (>16%). For **1**, the presence of two additional methylene protons at the glycosidic linkage allows more conformational information to be obtained. Although only qualitatively, the observed NOEs are shown in Table 4 in comparison with the predicted ensemble average distances. A good match is observed between the two sets of data. However, the analysis presented herein deserves some comments: the presence of a conformational equilibrium has been determined. Nevertheless, it has to be stated, following Neuhaus and Williamson,[14] that the ability to fit NOE data using predicted conformations cannot be taken to mean that those conformations are necessarily those that are present; other choices might well fit the NOE data also.

In conclusion, all the NMR results (NOE and *J* data) have allowed us to demonstrate a different conformational behavior of *C*-mannobioside with respect to its *O*-analogue. To summarize, the global minima of **1** and **2** adopt *exo*-anomeric conformations around ϕ, but the orientations around the aglyconic bond ψ are rather different between both compounds. It is noteworthy that the presence of conformer C for **1**, which has a conformation not favored by the *exo*-anomeric effect, with a torsional variation of 120° upon the ϕ angle, has never been observed for α-*O*-glycosides and is very unusual for β-*O*-glycosides.[16] Therefore, *C*-glycosides may also display significant variations, not only around ψ as mainly

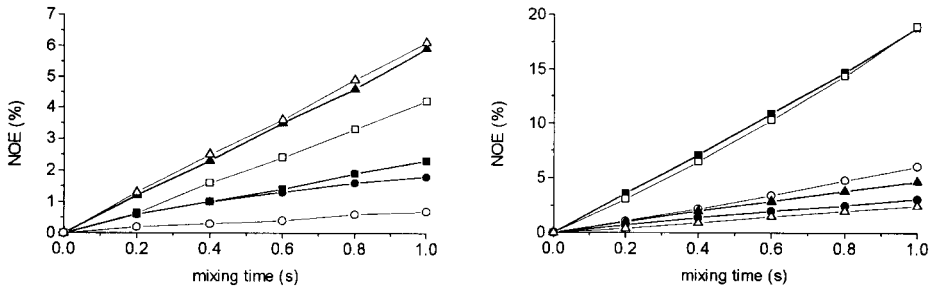

Figure 4. Experimental and calculated NOE curves for compound **1**. Thick lines with filled symbols: experimental curves. Open symbols: calculated curves. Left: ■,□: H2/H2′; ●,○: H2/H5; ▲,△: H2/H1; right: ■,□: H2/H1′ + H3; ●,○: H1/H1′; ▲,△: H1/H5.

Table 4. Ensemble average distances $\langle r^{-6}\rangle^{-1/6}$ and observed NOEs for the methylene protons. For the observed NOEs of **1**, the first letter indicates the intensity to H7pro*S* and the second one to H7pro*R*. For compound **3**, only one proton exists. Strong, medium, and weak NOEs are denoted by s, m, and w, respectively.

	Theoretical H7pro*S* $\langle r^{-6}\rangle^{-1/6}$	Theoretical H7pro*R* $\langle r^{-6}\rangle^{-1/6}$	Observed NOEs **1** D_2O	Observed NOEs **1** $[D_6]$DMSO	Observed NOEs **1** MeOD	Observed NOEs **1** $[D_5]$Pyr	Observed NOEs **3**
H1	2.7	3.6	ms/–	mw/–	m/vw	s/vw	mw
H2′	3.2	2.4	–/s	–/s	–/s	–/s	s
H3′	2.5	2.7	m/mw	m/w	m/w	ms/m	s
H5′	2.2	2.7	s/w	s/–	s/–	s/–	ms
H4	2.4	2.6	m/m	mw/m	w/m	m/m	s

observed for β-*C*-lactosides[5] but also around ϕ. Kishi and coworkers have questioned the importance of the *exo*-anomeric effect as the major factor determining why *O*-glycosides adopt their particular conformation.[17] Our results suggest that in the absence of stereoelectronic stabilization, conformations which are not consistent with the *exo*-anomeric disposition may be adopted. This fact indicates that the *exo*-anomeric effect is indeed an important factor in determining the conformational behavior of *O*-glycosides. In addition, the finding that three areas of the conformational maps are populated in solution demonstrates that **1** is much more flexible than **2**.

Conformational features of compound 1 in MeOD, [D$_6$]DMSO, and [D$_5$]Pyr: Oligosaccharide conformational analysis is sometimes performed in solvents other than water, such as DMSO, in order to demonstrate the degree of flexibility of the glycosidic linkage and to mimic the binding site of biomolecular receptors.[18] On this basis, additional information on the existence of extensive conformational flexibility for **1**, as well as a different conformational behavior with respect to **2**, was inferred from the dependence of the relevant NMR parameters on the solvent employed for the NMR measurements.

Thus, vicinal proton–proton coupling constants (Table 2) as well as NOEs through T-ROESY and NOESY (Tables 3 and 4) measurements were obtained for **1** in MeOD, [D$_6$]DMSO, and [D$_5$]Pyr solutions. It was observed that the relevant interbridge couplings do not strongly depend on the solvent. This fact seemed to indicate that the conformational equilibrium is not significantly affected by solute–solvent interactions, in contrast with the observations reported for β-*C*-glycosides.[5] The major differences are observed between [D$_5$]Pyr and D$_2$O. $^3J_{H1'-H7pro\mathit{S}}$ and $^3J_{H2-H7pro\mathit{R}}$ values are larger in [D$_5$]Pyr than in D$_2$O, while $^3J_{H1'-H7pro\mathit{R}}$ and $^3J_{H2-H7pro\mathit{S}}$ values are somehow smaller. These numbers seem to indicate that the population of conformer A increases in [D$_5$]Pyr compared to D$_2$O. The observed differences in [D$_6$]DMSO and MeOD compared with the D$_2$O values are always smaller than 0.8 Hz, indicating a minor change in the respective populations through minima A, B, and C, although minimum B seems to be slightly more populated in these two solvents.

These observations were substantiated by NOE values recorded in these solvents. Tables 3 and 4 show the relevant proton–proton contacts. It can be observed that those NOEs which correspond to the proton–proton distances, which are closer in conformer A, are relatively stronger in [D$_5$]Pyr than in the other two solvents. This fact indicates again that the population of conformer A increases in [D$_5$]Pyr with respect to D$_2$O, [D$_6$]DMSO or MeOD. On the other hand, the relative NOEs are similar in the latter three solvents; again, this indicates a similar conformational distribution to that described above for D$_2$O, with a slight increase in the population of conformer B. According to the MM3* calculations, the solvation energies in water increase in the order A < B < C. Although merely qualitative, this fact could explain the higher population of conformers A and B in nonaqueous solvents.

Conformational features of compound 3 in aqueous solution: According to the results described above for **1**, steric and electrostatic factors determine the conformational behavior of **1** in solution. It is well known that the presence of hydroxy groups may alter the balance of these types of factors within the molecule.[19] In order to obtain information about which factors determine the relative orientation of the glycosidic linkages, a conformational analysis of **3** was also carried out. In the first step, molecular mechanics calculations with the MM3* force field were used. The minima described above for **1** were taken as starting structures to find the corresponding conformers of **3**. In order to assign the chirality of the interglycosidic CHOH group, a combination of *J* and NOE data was recorded, following a similar protocol to that described above for **1**, and it was determined that the CHOH group has the *S*-configuration. For the calculations, two different conditions were employed. In the first one, the GB/SA solvent model for water[12] was used. Then the calculations were repeated with a bulk dielectric constant of 78 D. The influence of the dielectric constant value used was inferred from the obtained results. In the first case, with the continuum solvent model, conformer C was the most stable one, followed by conformer A ($\Delta E = 8.2$ kJ mol^{-1}). Conformer B was destabilized by 14.7 kJ mol^{-1}. On the other hand, for $\varepsilon = 80$ debyes, conformer A was the global minimum, while the relative steric energy values for C and B were 3.9 and 11.2 kJ mol^{-1}, respectively. In both cases, minor differences in the corresponding torsion angles were found. These results indicate that the major conformer found for **1**, minimum B, seems to be rather more destabilized when the bridge carbon is substituted by a hydroxy group. According to the calculations, regions A and C should dominate the probability distribution. This result is again in sharp contrast with the results reported for the natural compound **2**.

In a second step, molecular dynamics simulations with the MM3* force field and the GB/SA solvent model for water were carried out. Three different trajectories were obtained by taking the different minima as starting structures. The obtained trajectory starting from minimum C remained at the same region during the 3 ns simulation. On the other hand, when the dynamics calculations started from either minimum A or B, the trajectories were basically identical and showed several transitions between these two conformational regions. Therefore, according to the simulations, the energy barrier between minima A and B (around ψ) is smaller than that existing between this area and minimum C (around ϕ). In comparison to the simulation described above for **1**, it seems that the energy barrier around ϕ increases upon OH-substitution at the α-carbon. As a test to predict the conformational behavior of the *R*-diastereomer of **3**, single-point MM3* calculations were also performed. The energy values obtained predict that now conformer B should be the most populated one (60%), followed by C (35%), and finally A (5%).

Nevertheless, in order to obtain reliable conformational information, the validity of the calculations were tested using experimental NMR measurements of vicinal proton–proton coupling constants and NOEs for **3**. Both H7 couplings to H1′ and H2 have the same value, namely, 5.3 Hz, which indicates

0947-6539/99/0502-0446 $ 17.50+.50/0 *Chem. Eur. J.* **1999**, *5*, No. 2

that a single conformer cannot explain the experimental values (see Table 2). Although many combinations[14] may explain the observed data, a near-identical population distribution between conformers A and C, with a fairly small contribution (<10%) of conformer B, is in agreement with the experimental values. In addition, this assumption was verified by NOE analysis. Indeed, the presence of strong H2/H2′, H7/H3′, and H7/H5′ can only be explained by the presence of an important population of conformer C. Medium H1/H1′ and weak H1/H2′ NOEs are also exclusive to the presence of conformer C. In addition, the strong H4/H7 is indicative of the existence of conformer A. Moreover, the absence of the B-exclusive H1/H5′ NOE, clearly observed in **1**, indicates that the population of this conformer is greatly decreased upon hydroxy substitution on the bridged-carbon atom to give **3**. In this case, the MD simulations predict a larger contribution of conformer B than that found experimentally.

Therefore, our results clearly confirm that the flexibility around the glycosidic linkages of both β- and α-*C*-glycosides may be easily determined by NMR spectroscopic experiments. In addition, the conformational changes observed upon variation of the solvent or *C*-hydroxy substitution also reflect the small energy barriers between the different energy regions. Thus, conformations different from the major one existing in solution may be bound by the binding site of proteins without major energy conflicts. These results, along with those previously obtained by us for *C*-lactose (with a β-glycosidic linkage), are important for drug design. For the binding of a flexible compound to a protein, usually one of the existing conformations should be selected out of the ensemble.[20] Therefore, a negative binding entropy would be expected, thus decreasing the energy of binding.[21] Consequently, the flexibility of *C*-disaccharides may be a limitation in the use of *C*-disaccharides as therapeutic agents. Nevertheless, these compounds are still excellent probes for the study of the binding sites of proteins and enzymes.[16a, 22] They may also serve as test compounds to compare conformational properties of oligosaccharides.

Experimental Section

Molecular mechanics and dynamics calculations: Molecular mechanics and dynamics calculations were performed using the MM3* force field as implemented in Macromodel 4.5.[23] ϕ is defined as H1′-C1′-C7-C2 and ψ as C1′-C7-C2-H2, that is, the atoms of the nonreducing end are primed. Only the *gg* orientation of the lateral chain was used for the α-Man moieties. Separate calculations for a dielectric constant $\varepsilon = 80$ debyes and for the continuum GB/SA solvent model were performed.[12] First, potential energy maps were calculated for the disaccharides: relaxed (ϕ,ψ) potential energy maps were calculated as previously described.[24] Four initial geometries were considered, cc, cr, rr and rc, obtained by combining the positions r (reverse clockwise) and c (clockwise) for the orientation of the secondary hydroxy groups of both pyranoid moieties. The first character corresponds to the nonreducing moiety, and the second one to the reducing moiety. In total, 1600 conformers were calculated for every disaccharide and both dielectric conditions. The previous step involved the generation of the corresponding rigid residue maps by using a grid step of 18°. Then, every ϕ,ψ point of this map was optimized using the 200 steepest descent steps, followed by 1000 conjugate gradient iterations. From these relaxed maps, adiabatic surfaces[7] were built, and the probability distributions were calculated for each ϕ,ψ point according to a Boltzmann function at 303 K.

The energy minima structures (A, B, and C) were used as starting geometries for molecular dynamics (MD) simulations[25] at 300 K, with the GB/SA solvent model, and a time step of 1 fs. The equilibration period was 100 ps. After this period, structures were saved every 0.5 ps. The total simulation time was 3 ns for every run. Average distances between intraresidue and interresidue proton pairs were calculated from the dynamics simulations.

NMR spectroscopy: NMR experiments were recorded on Varian Unity 500 and Bruker AMX-600 spectrometers, with an approximately 3 mg mL^{-1} solution of the disaccharides at different temperatures. Chemical shifts δ are reported against the residual HDO signal ($\delta = 4.71$) and external TMS ($\delta = 0$) as references. The double-quantum filtered COSY spectrum was obtained with a data matrix of 256×1 K to digitize a spectral width of 2000 Hz. 16 scans were used with a relaxation delay of 1 s. The 2D TOCSY experiment was performed using a data matrix of 256×2 K to digitize a spectral width of 2000 Hz; 4 scans were used per increment, with a relaxation delay of 2 s. MLEV 17 was used for the 100 ms isotropic mixing time. Data from the one-bond proton–carbon correlation experiment were collected in the ^{1}H-detection mode with the HMQC sequence and a reverse probe. A data matrix of 256×2 K was used to digitize a spectral width of 2000 Hz in F_2 and 10000 Hz in F_1. Four scans were used per increment with a relaxation delay of 1 s and a delay corresponding to a *J* value of 145 Hz. A BIRD pulse was used to minimize the proton signals bonded to ^{12}C. ^{13}C decoupling was achieved by the WALTZ scheme.

NOESY experiments were performed with the selective 1D double-pulse field-gradient spin echo module, using four different mixing times, namely 150, 300, 450, and 600 ms. 2D NOESY, 2D-ROESY, and 2D-T-ROESY experiments were also performed with the same mixing times, and with 256×2 K matrices.

NOE calculations: NOESY spectra were simulated according to a complete relaxation matrix approach, following the protocol previously described,[24] with four different mixing times (between 150 and 600 ms). The spectra were simulated from the average distances $\langle r^{-6} \rangle_{kl}$ calculated from the relaxed energy maps at 303 K. Isotropic motion and external relaxation of 0.1 s^{-1} were assumed. A τ_c of 45 ps was used to obtain the best match between experimental and calculated NOEs for the intraresidue proton pairs (H1′/H2′ and H1/H2).

All the NOE calculations were automatically performed by a program written by the authors and available from them on request.[24]

Acknowledgments

Financial support by DGICYT (Grant PB96-0833) and by Mizutani Glycoscience Foundation is gratefully acknowledged. J.F.E. thanks Ministerio de Educacion y Ciencia for a FPU fellowship.

[1] *Chemistry of C-glycosides* (Eds.: W. Levy, D. Chang), Elsevier, Cambridge, **1995**.
[2] B. A. Johns, Y. T. Pan, A. D. Elbein, C. R. Johnson, *J. Am. Chem. Soc.* **1997**, *119*, 4856–4865.
[3] a) A. Wei, K. M. Boy, Y. Kishi, *J. Am. Chem. Soc.* **1995**, *117*, 9432–9437; b) Y. Wang, P. G. Goekjian, D. V. Ryckman, W. H. Miller, S. A. Babirad, Y. Kishi, *J. Org. Chem.* **1992**, *57*, 482–489.
[4] J. F. Espinosa, M. Martín-Pastor, J. L. Asensio, H. Dietrich, M. Martín-Lomas, R. R. Schmidt, J. Jiménez-Barbero, *Tetrahedron Lett.* **1995**, *36*, 6329–6332.
[5] J. F. Espinosa, F. J. Cañada, J. L. Asensio, M. Martín-Pastor, H. Dietrich, M. Martín-Lomas, R. R. Schmidt, J. Jiménez-Barbero, *J. Am. Chem. Soc.* **1996**, *118*, 10862–10871.
[6] O. Jarreton, T. Skrydstrup, J.-M. Beau, *J. Chem. Soc.Chem. Commun.* **1996**, 1661–1662; O. Jarreton, T. Skrydstrup, J.-F. Espinosa, J. Jiménez-Barbero, J.-M. Beau, *Chem. Eur. J.* **1999**, *5*, 440; previous paper in this issue.
[7] T. Peters, B. M. Pinto, *Curr. Opin. Struct. Biol.* **1996**, *6*, 710–720.

[8] S. W. Homans, A. Pastore, R. A. Dwek, T. W. Rademacher, *Biochemistry* **1987**, *26*, 6649.
[9] T. Peters, *Liebigs Ann. Chem.* **1991**, 135 – 141.
[10] a) H. Paulsen, T. Peters, V. Sinnwell, R. Lebuhn, B. Meyer, *Liebigs Ann. Chem.* **1984**, 951; b) C. J. Edge, U. C. Singh, R. Bazzo, G. L. Taylor, R. A. Dwek, T. W. Rademacher, *Biochemistry* **1990**, *29*, 1971 – 1974.
[11] a) R. U. Lemieux, S. Koto, D. Voisin, *Am. Chem. Soc. Symp. Ser.* **1979**, *87*, 17 – 29; b) G. R. J. Thatcher, *The Anomeric Effect and Associated Stereoelectronic Effects*, American Chemical Society, Washington, DC, **1993**.
[12] W. C. Still, A. Tempczyk, R. C. Hawley, T. Hendrickson, *J. Am. Chem. Soc.* **1990**, *112*, 6127 – 6128.
[13] C. A. G. Haasnoot, F. A. A. M. de Leeuw, C. Altona, *Tetrahedron* **1980**, *36*, 2783. Higher order effects were taken into account by simulation of the spectrum using gNMR 3.6.
[14] D. Neuhaus, M. P. Williamson, *The Nuclear Overhauser Effect in Structural and Conformational Analysis*, VCH, New York, **1989**.
[15] K. Stott, J. Stonehouse, J. Keeler, T.-L. Hwang, A. J. Shaka, *J. Am. Chem. Soc.* **1995**, *117*, 4199.
[16] a) J. F. Espinosa, E. Montero, A. Vian, J. L. Garcia, H. Dietrich, M. Martín-Lomas, R. R. Schmidt, A. Imberty, J. Cañada, J. Jiménez-Barbero, *J. Am. Chem. Soc.* **1998**, *120*, 10862 – 10871; b) C. Landersjo, R. Stenutz, G. Widmalm, *J. Am. Chem. Soc.* **1997**, *119*, 8695 – 8701.
[17] T.-C. Wu, P. G. Goekjian, Y. Kishi, *J. Org. Chem.* **1987**, *52*, 4819 – 4823.
[18] Z. Y. Yan, B. N. N. Rao, C. A. Bush, *J. Am. Chem. Soc.* **1987,** *109*, 7663 – 7669.
[19] J. F. Espinosa, H. Dietrich, M. Martín-Lomas, R. R. Schmidt, J. Jiménez-Barbero, *Tetrahedron Lett* **1996**, *37*, 1467 – 1470.
[20] M. S. Searle, D. H. Williams, *J. Am. Chem. Soc.* **1992,** *114*, 10690 – 10697.
[21] D. R. Bundle, N. M. Young, *Curr. Opin. Struct. Biol.* **1992**, *2*, 655 – 660.
[22] J. F. Espinosa, F. J. Cañada, J. L. Asensio, H. Dietrich, M. Martín-Lomas, R. R. Schmidt, J. Jiménez-Barbero, *Angew. Chem.* **1996**, *108*, 323 – 326; *Angew. Chem. Int. Ed. Engl.* **1996**, *35*, 303 – 306.
[23] F. Mohamadi, N. G. J. Richards, W. C. Guida, R. Liskamp, C. Caufield, G. Chang, T. Hendrickson, W. C. Still, *J. Comput. Chem.* **1990**, *11*, 440 – 467.
[24] J. L. Asensio, J. Jiménez-Barbero, *Biopolymers* **1995**, *35*, 55 – 73.
[25] R. J. Woods, *Curr. Opin. Struct. Biol.* **1995**, *5*, 591 – 598.

Received: May 25, 1998 [F1168]

0947-6539/99/0502-0448 $ 17.50+.50/0